Rotor Design Optimization of Squirrel Cage Induction Motor - Part II: Results Discussion

Mauro Di Nardo[1], Alessandro Marfoli[1], Michele Degano[1], Chris Gerada[1], Wenliang Chen[2]
[1] University of Nottingham, Nottingham, UK, mauro.dinardo4@nottingham.ac.uk
[2] ABB Corporate Research Västerås, Sweden

***Abstract*—The rotor slot geometry of a squirrel cage induction motor plays the most important role in defining the torque-speed characteristic when the power supply is directly provided by the main grid. In this paper it is shown how the rotor slot geometry can be optimised to satisfy different electromechanical requirements, depending on specific applications. This work, the second of two companion papers, briefly recalls the novel systematic approach, proposed in Part I, to perform the optimization of squirrel cage induction motors. Here, the optimization results achieved satisfying a wide spectrum of requirements are analysed in depth. Furthermore, the trade-off among the several performance indexes and their correlation with the geometrical parameters is discussed. The possible advantages and disadvantages of adopting a copper cage is also quantified for all possible performance requirements. The influence of the motor thermal behaviour and harmonic losses on the overall performance are also discussed allowing to validate the proposed design optimization procedure and its results. The outcomes of this work are opening to new design approaches that enable to optimise the performance of one of the most popular electrical machines adopted in industry, the squirrel cage induction motor.**

***Index Terms*—Efficiency Improvement, Finite Element Analysis, Induction Motor, Multi-Objective Optimization, Squirrel Cage, Rotor Slot Design.**

I. Introduction

Nowadays there are two main factors behind the ever increasing interest towards high efficient motors. Being the electric motors one of the major user of electric energy [1], the first one is the need of mitigating the ever increasing energy demand with a significant reduction of the energy consumption, aimed at minimising CO_2 emissions. The second one is the economical advantage of employing high efficiency motors. As a matter of fact, the operating cost of an industrial motor over its life represents approximately 95% of the total cost of ownership. Therefore, the higher initial capital cost corresponds to a considerable saving opportunity in terms of operating cost, especially for large motors [1]. The international standard IEC 60034-30-1 defines four different classes of efficiency, as reported in Fig.1. The minimum efficiency requirement increases with the power rating and the potential efficiency increment from one class to the next is higher for small power rating with respect to powerful machines. Fig.1 also reports a further efficiency level named IE5, which is envisaged to be incorporated into the next edition of this standard. The corresponding efficiency is calculated imposing a 20% reduction of the losses with respect to IE4 machine. Since 2017, IE3 is the legally specified minimum efficiency in

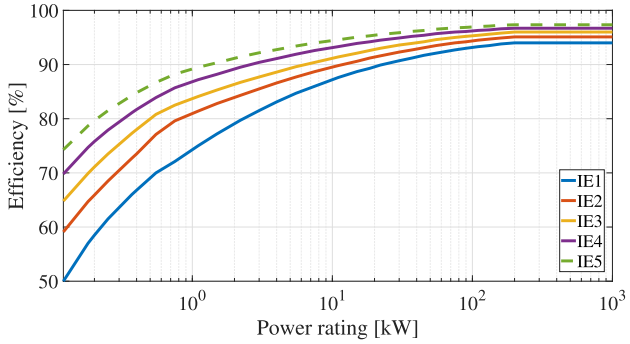

Fig. 1: Efficiency levels defined by IEC 60034-30 for a 4-poles, 50Hz SCIM [3].

Europe for direct fed motors having power ratings from 0.75 kW up to 375 kW. Similar regulations imposing a minimum IE3 (or equivalent) efficiency level has been introduced in US and China in 2010 and 2016, respectively [2]. Improving the performance of a squirrel cage induction motor (SCIM), either rating or efficiency, can be achieved modifying several design variables or choices. The ones having the highest impact are:

- increase the amount of active materials;
- use high performance magnetic materials;
- lower the operating temperature improving the heat transfer between the active parts and the external ambient;
- optimize the stator and rotor geometries;
- adopt copper squirrel cage.

Techniques for improving SCIM efficiency based on the modifications of existing machine's designs with the minimum economical impact for motor manufacturers have been one of the key topic in this field [4], [5]. Core axial lengthening and employment of better magnetic material [6], [7] are the most effective approaches for increasing the SCIM efficiency using existing stator and rotor laminations. Although the first one, it has been successful implemented in recent years to modify standard efficiency SCIMs in IE3 machines, it has shown several limitations [8]. The length of the motor must be compatible with the external frame of the original motor or with other available frames. Furthermore, the design modification has to comply with the other requirements. A design change intended to improve the efficiency could lead to a violation of other performance indexes, such as minimum starting, pull-up and breakdown torques [5]. Therefore, this design approach adopted to incrementally increase the efficiency 1) does not guarantee that the efficiency improvement is reached with the minimum active material increment and 2) becomes ineffective when large efficiency gains are required or when the IE4 class

is the target. In general, the selection of the efficiency improvement design approach is merely economical, and it has to be done comparing the cost of the design modification (increased axial length or improved magnetic material) with respect to the total cost required for a complete machine redesign (including the cost of the new punching tool). Another design option to improve the efficiency of SCIMs is the adoption of copper rotor cage in substitution of the more common aluminium cage [9]. Traditionally copper rotor cages are employed in medium-high voltage motors and use pre-manufactured bars inserted in the rotor slot and brazed to the end-rings [10]. Small-medium power SCIMs manufactured with fabricated copper bars have never been considered an economically viable solution due to its high-labor cost. However, the improvement of the copper die-cast technologies (mainly the mould materials) in the last decade has led to the possibility of manufacturing die-cast copper cage rotors as it has been traditionally done with aluminium [11]. The adoption of copper cages has a threefold effect on the SCIM's efficiency. A direct improvement of the latter due to the lower rotor joule losses, and two indirect ones due to the consequent lower stator joule losses, and lower rotor operating temperatures [12]. The straight substitution of the rotor cage material, from aluminium to copper, without modifying the rotor lamination geometry leads to a lower rotor resistance, thus improving the efficiency. However, the starting torque and the related current are deteriorating [9]. Efficiency improvements cannot be achieved without affecting the starting performance, unless a redesign of the lamination is carried out [7]. In addition, the complete redesign allows to achieve higher efficiency improvement with respect to the simple substitution of the cage material, thanks to the better exploitation of the latter [7]. Considering all the above, it can be deduced that the SCIM design is a complex multi-objective optimization problem [13]. In fact, more than one objective has to be considered during the design process and most of them show an inherently competitive behaviour.

Part I of this work has addressed the various challenges of implementing an automatic design optimization procedure of a direct-fed SCIM. The latter has been defined in terms of performance evaluation method, performance indexes to be optimized and geometrical variables defining the research space. Although the proposed optimization strategy is general and so suitable to design the whole machine, in this work it has been applied to optimize the rotor slot geometry being this the most influential factor in defining the SCIM behaviour. The aims of this second part of the study are the following:

- evaluate the trade-off among the performance indexes;
- investigate the influence of the rotor bar geometry with respect to the SCIM performance;
- asses the capability of an optimum bar shape in satisfying a wide spectrum of requirements;
- quantify advantages and eventual drawbacks of adopting a copper cage.

Sections II reports the optimization results obtained adopting aluminum and copper cage material. Section III presents the analysis of the optimized bar geometries along the performance for all the operating speed range. The validation of the optimization method is presented in section IV where a coupled electromagnetic-thermal analysis of the optimal solutions is reported along with the results of more accurate time-step finite element analysis (FEA).

II. Optimizations results

Starting torque (T_{start}) and rated efficiency (η_{rated}) are selected as performance indexes to maximize. The ratio between starting and rated currents ($k_{I,max} = I_{start}/I_{rated}$) is selected as constraint. The rotor slot geometry to be optimized is described by six variables as shown in Fig. 2. The latter is based on a generalized per unit parametrization of the classical Boucherot bar, as fully described in Part I. The bridge thickness (b) has been kept fixed and equal to the minimum allowed by manufacturing considerations (0.5 mm). The method for the evaluation of the starting and rated performance, along with the specifications of the considered SCIMs, have been detailed in the first part of these two companion papers and they are not reported here for the sake of brevity. As mentioned in first part of this work, the rotor design is carried out using a population-based multi-objective stochastic optimization algorithm (NSGA-II) evaluating a total of 10000 solutions. The following sub-sections are presenting the results of the optimizations carried out considering A) an aluminium cage and B) a copper cage. For each material, the rotor geometry has been optimized considering different maximum current ratios as well as constant and variable rotor slot surface. The last sub-section (C) reports the comparison between the results obtained optimizing the aluminium and the copper cage.

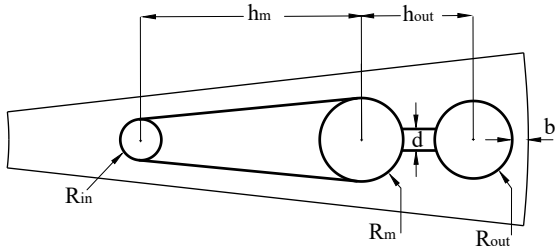

Fig. 2: Parametrization of rotor bar.

A. Aluminium cage

The optimization results are reported in Fig. 3a), where the Pareto fronts are obtained considering maximum current ratios $k_{I,max}$ ranging from 4.4 to 9.4. The markers' colour represent the real current ratio k_I of each motor design. Analysing these results, obtained for a fixed slot area (A^*_{slot}), the following considerations can be drawn.

- Given a certain $k_{I,max}$, the best performance are achieved by designs featuring a real current ratio k_I close to the imposed limit; this confirms the crucial rule of the starting current in defining the overall performance.
- All three considered performance indexes show a competitive behaviour, i.e. no figure of merit can be improved without worsening another.
- For a given starting torque, higher current ratio determines an improvement of the rated efficiency; this improvement is higher in the high starting torque region.

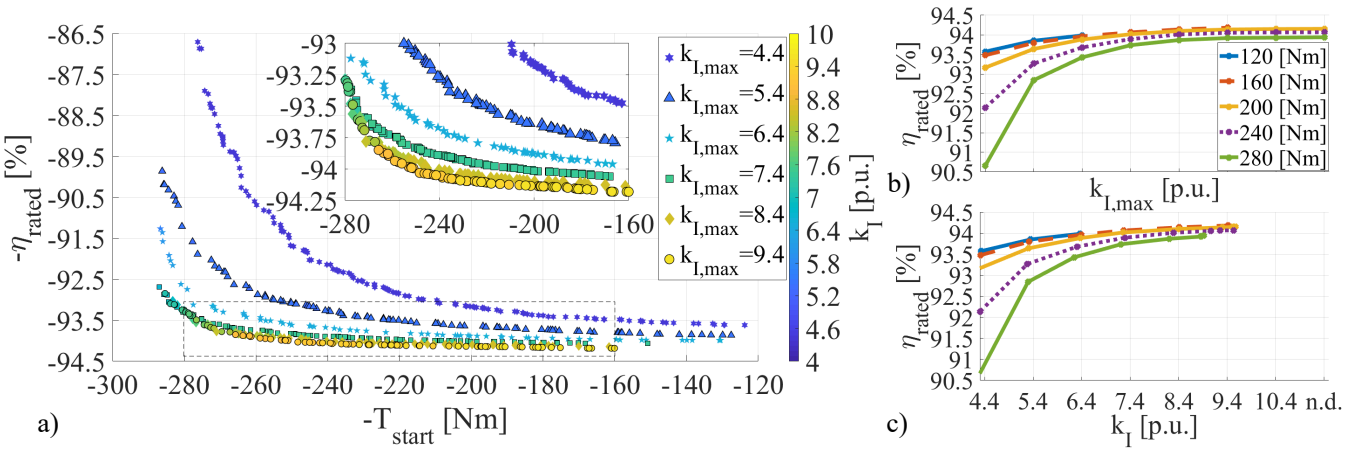

Fig. 3: Aluminium cage optimization results with constant slot area: a) Pareto fronts obtained with different current ratio limits; b,c) rated efficiency of the optimized machines as function of the current ratio limit (b) and current ratio (c) for different value of starting torque.

- A wide range of starting torques can be obtained for any current ratio limit and such range is almost independent of the constraint value $k_{I,max}$.
- The Pareto fronts are wider in term of starting torque with respect to the rated efficiency; for example, considering the current ratio 5.4, an improvement of 100% of the starting torque (from 140 to 280 Nm) implies a reduction of the rated efficiency of only 2.8% (from 93.85 to 91.21%).
- The release of the starting current constraint leads to more flat Pareto fronts; therefore the rated efficiency degradation in the high starting torque region is less than the one encountered for lower current ratio limits.
- For a given starting torque, as the current ratio limit increases, the rate of the efficiency improvement decreases until it becomes almost null.

The latter behaviour is highlighted in Fig. 3b) where the results of the optimizations are reported by plotting the efficiency against k_I. In the figure are also included the results obtained with a higher current ratio limit (k_I =10.4) and without imposing any constraint (reported as n.d. on the rightmost part of the figure). In Fig. 3b), it can be notice that increasing the maximum current ratio above a certain value does not lead to any efficiency improvement. Fig. 3c) shows the rated efficiency of the optimal machines as function of the real current limit k_I; it is worth to notice that even if the current ratio constraint is relaxed above k_I =9, the real ratio between the starting and the rated current does not increase.

Slightly better results are always achieved if the rotor slot area is let free to vary during the optimization, as shown in Fig. 4. The latter compares the Pareto fronts obtained considering three maximum current ratios (5.4, 7.4 and 9.4) with constant (A^*_{slot}) and variable slot area; the color scale indicates the relative variation of the slot area (ΔA_{slot}) with respect to the considered initial value (A^*_{slot}). Designs having high current ratios feature better efficiency improvements especially for bar geometries producing low starting torques. Considering the lowest current ratio limit (5.4), the optimal slot area is always bigger than the initial value. In the best case scenario, an increment of the slot area (ΔA_{slot}) of 10% leads to an efficiency improvement of only 0.2%. For medium-high

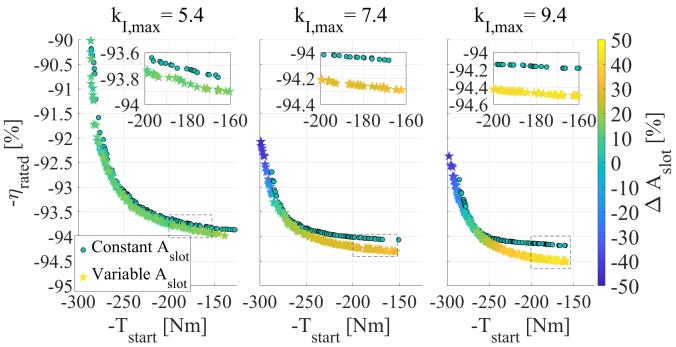

Fig. 4: Aluminium cage optimization results with variable slot area: Pareto fronts obtained with different current ratio limits; the slot area deviation from the rated one is shown with the color scale.

current ratios (7.4-9.4), the optimal slot area increases as the starting torque decreases, with values lower than the initial one in the high starting torque region and vice versa. Considering the results achieved constraining the maximum current ratio to 9.4, for the starting torque T_{start} =160 Nm, a 40% increment of the slot area produces a 0.3% improvement in the rated efficiency.

B. Copper cage

Similar trends have been obtained optimizing the slot geometry hosting a copper bar. Fig. 5a) shows the Pareto fronts achieved imposing three different current ratio limits (5.4, 7.4 and 9.4) maintaining the same slot surface (A^*_{slot}). It is worth noting that the starting torques range of variability is almost as wide as the one obtained considering an aluminium cage with the same slot surface (i.e. 120-300 Nm). Consequently, it can be deduced that for a certain starting torque and maximum current ratio, the rotor slot geometry optimized considering a copper bar will be different with respect to the optimal geometry obtained with aluminium bars. This aspect and its implications will be further discussed in the next section.

Removing the constant rotor slot area constraint, the results marginally improve, as can be noticed in Fig. 5b). The latter is analogous to Fig. 4 for the copper cage. For any considered starting torque and current ratio limit, letting the slot area free to vary always leads to a better efficiency, with the same

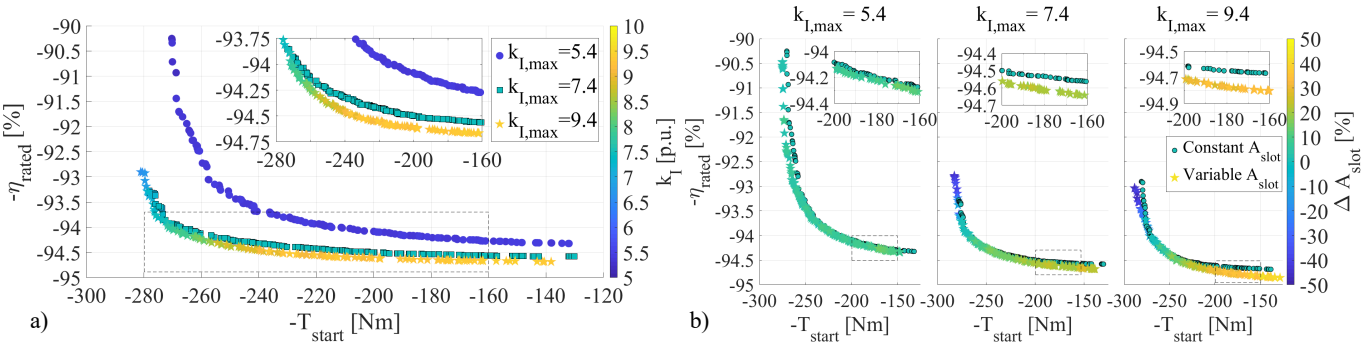

Fig. 5: Copper cage optimization results for different current ratio limits: a) with constant slot area and b) with variable slot area.

behaviour with respect to the aluminium cage rotor. Also in this case, the efficiency improvement increases as the starting torque decreases and the current ratio constraint is relaxed. In terms of optimal slot area, the trends are similar to the ones obtained optimizing the aluminium bar geometry: higher starting torques are achieved reducing the slot surface and vice versa. The optimal slot area becomes equal to the reference one (A^*_{slot}) in the proximity of the point of contact between the two Pareto fronts.

It is worth to underline that the highest efficiency improvements achieved optimizing the rotor slot area of a copper cage are smaller than the one obtained with the aluminium cage. This observation is strictly related to the fact that the reference slot area considered for the copper bar is the same of the aluminium one.

C. Cage material comparison

Fig. 6a) compares the optimization results obtained considering both aluminium and copper bars for different current ratio limits for the same rotor slot area. The copper bars outperform the aluminium ones in term of efficiency in the medium-low starting torque region. The efficiency gain increases as the starting torque decreases reaching a maximum of 0.5% at $T_{start} = 160$ Nm and $k_{I,max} = 9.4$. In the high starting torque range, the copper and aluminium Pareto fronts intersects each other, and efficiency wise it is not anymore convenient to adopt a copper cage. The lower resistivity of the copper with respect to the aluminium, the fact that both optimizations feature the same slot surface and current ratio limit justify this trend. On one hand, the lower copper resistivity leads to an increased efficiency for low starting torques SCIMs. On the other hand, higher starting torques can be achieved with a copper bar only at the expense of a lower efficiency. This behaviour will be commented in the next paragraph when the optimal geometries and the bar parameters variation, in term of resistance and inductance, will be presented. When the slot surface is unconstrained, the difference between the performance of the optimal aluminium and copper bars becomes smaller, as shown in Fig. 6b). Optimizing the geometry of a copper bar leads to a better efficiency with respect to the aluminium ones except for really high starting torques and lower current ratio limits. However, for a given maximum current ratio, the same starting torque requirement (e.g. 160 Nm) is achieved with a copper bar having a smaller slot cross section than the aluminium one, as depicted in the insets of Fig. 6b).

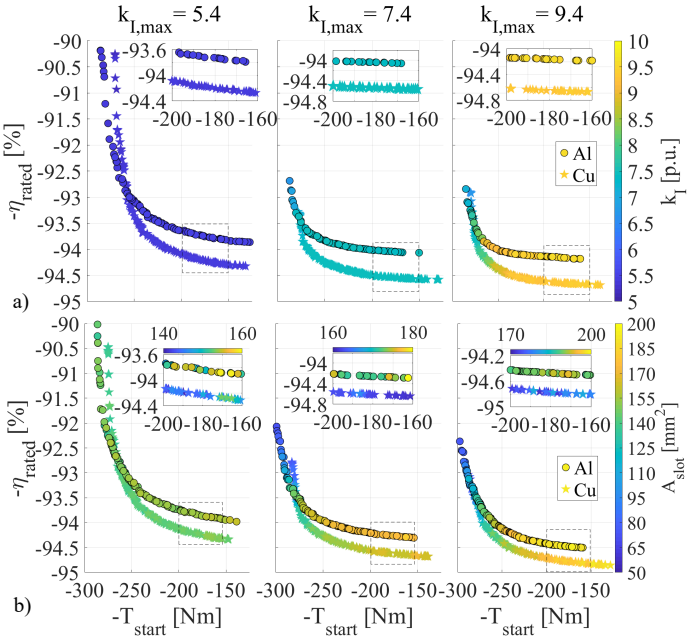

Fig. 6: Optimization results considering aluminium and copper cages obtained a) with constant slot area and b) with variable slot area for different current ratio limits.

It has to be underlined that the rotor slot geometry has been optimized considering the same temperature for both aluminium and copper cages as well as for the stator windings. This comparison is not completely fair because the lower rated joule losses of the cage the lower rotor temperatures are. This aspect will be investigated in detail is Section IV-A.

III. Analysis of the Optimized Machines

In this section the performance of a representative subset of optimal solutions are reported and commented for different operating points, along with the corresponding rotor slot geometries. The performance are evaluated with the EC featuring parameters determined via time harmonic FE simulations (TH-FE) adopting the contextual identification method. Three maximum current ratio have been chosen for further investigation, 5.4, 7.4 and 9.4 expressed in p.u.; for each of them four different solutions producing a starting torque of 160, 200, 240 and 280 Nm have been selected from the corresponding Pareto fronts where the slot area has been constrained to A^*_{slot}. Considering the same normalized starting current limits, an additional solution producing a starting torque of 160 Nm has

been picked from the Pareto front obtained unconstraining the slot surface. Fig. 7a), b) and c) show the torque-slip curves and the geometries of the selected optimal aluminium bars; Fig. 7d), e) and f) report the same results for the copper cage. The performance indexes and the geometrical parameters of the optimized aluminium slots with constant area in the $k_{I,max} - T_{start}$ plane, are shown in Fig. 8a) and b). Fig. 8c) shows the bar resistance and reactance in the same design plane for the rated, breakdown and starting conditions. Fig. 8d) and e) depict the rotor slot current density distributions in rated and starting operating points.

A. *Optimal rotor slots constraining the area*

Analysing Fig. 7) and Fig. 8) the following considerations can be drawn.

- Independently of the cage material and per unit starting current limit, high starting torques are achieved with bars featuring longer shapes; in particular, as the starting torque increases the length of the bar neck increases, while its thickness decreases. At the same time, as T_{start} increases also the radius of the bar external circle (R_{out}) increases and being the slot area constant follows a reduction of the area of the inner part of the cage. This is not true for very high values of $k_{I,max}$ where R_{out} first increases then decreases due to the fact that the geometries providing the highest efficiency converges to a drop shape. The described trends of the geometrical parameters can be clearly observed in Fig. 8a) when moving on the iso-$k_{I,max}$ lines.
- Comparing rotor slots optimized with the same cage material, it can be observed that the same starting torque can be achieved with bars having very different geometries. As the starting current constraint is relaxed (thus the efficiency increases), when considering solutions that provide the same T_{start}, the conductive material moves towards the external part of the rotor. In other words, as shown in Fig. 8b), the overall bar length (L) decreases (mainly due to the neck length h_m) as $k_{I,max}$ increases, while the radius of the external circle (R_{out}) becomes bigger. In the low starting torques region, when $k_{I,max}$ increases the bar shapes changes from being a Boucherout geometry, with a smaller head to a well proportioned Boucherot bar and finally to a drop-shape bar for the highest value of $k_{I,max}$. For medium values of T_{start}, the bars are always variants of the classical Boucherot geometry. In the very high starting torques region, the Boucherot geometry is taken to the extreme in terms of length, especially the neck's dimensions.
- The starting torque and rated efficiency for different $k_{I,max} - T_{start}$ values are summarized in Fig. 8b), along with the behaviour of the rated slip, breakdown torque and slip, pull-up torque and rated power factor. It can be noticed that the efficiency increase in the direction that goes from high-T_{start}/low-$k_{I,max}$ to low-T_{start}/high-$k_{I,max}$. Along the same direction, the rated slip decreases while the rated power factor, the breakdown torque and related slip increase. In other words, relaxing the starting current limit allows achieving higher breakdown torques and power factors. Consequently, it can be stated that, keeping constant the slot area, the optimization of the rated efficiency implies the maximization of both power factor and breakdown torque. An unexpected behaviour is exhibited by the slip value at breakdown in Fig.8b). Although the rated slip decrease for designs with higher efficiency, the breakdown slip is moving

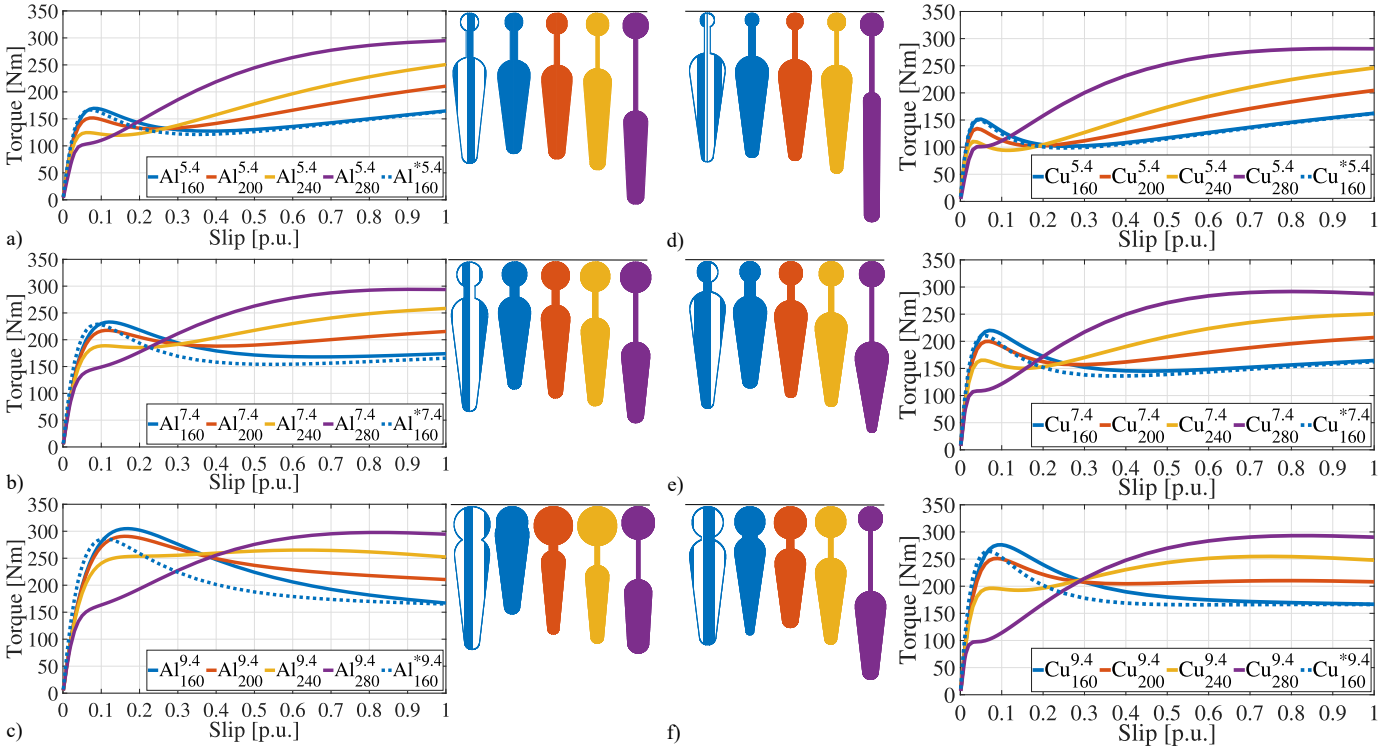

Fig. 7: Selected optimal slot geometries and their torque slip characteristics for different maximum current ratios obtained optimizing the aluminium cage (a, b, c) and the copper cage (d, e, f).

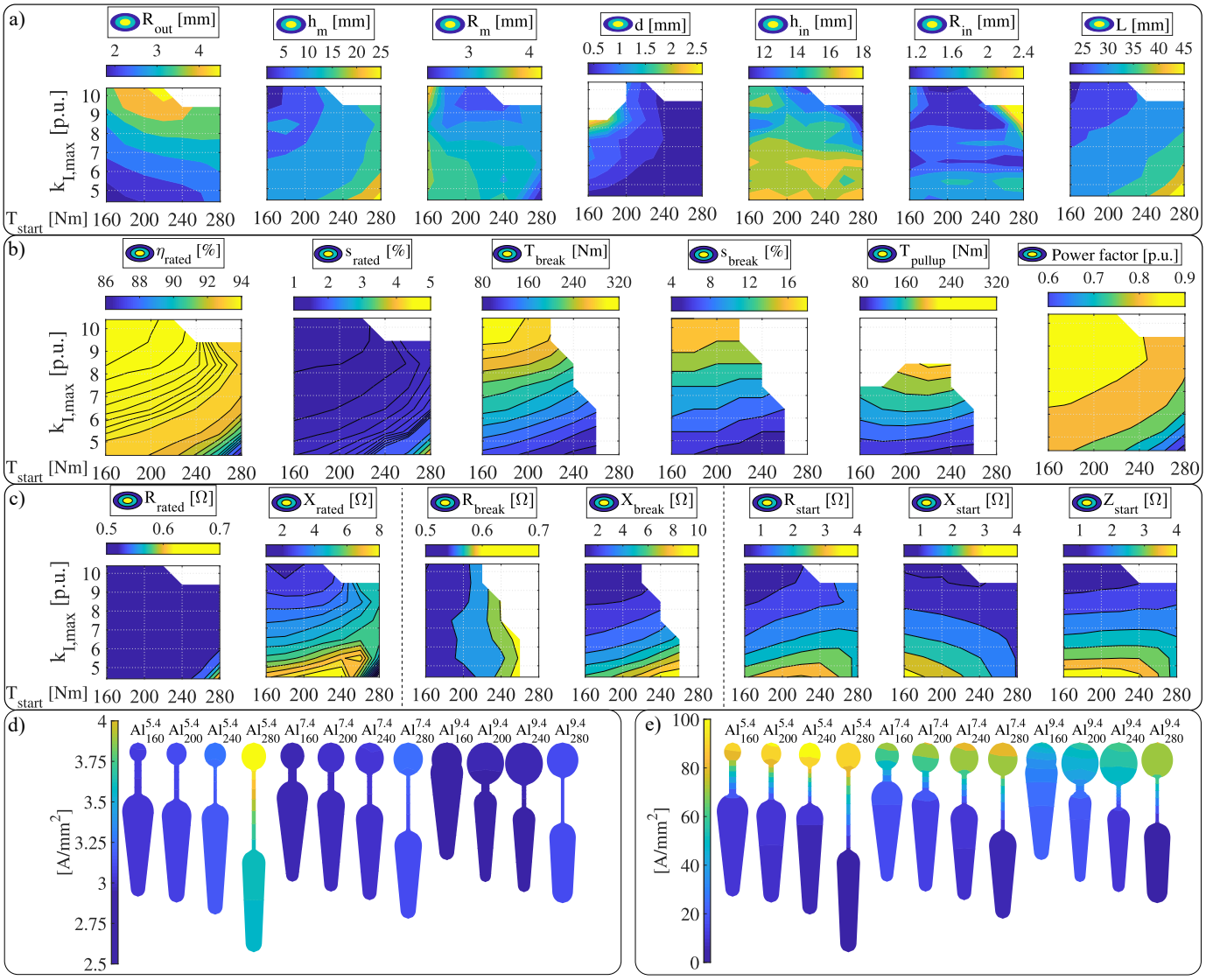

Fig. 8: Performance indexes a) and geometrical parameters b) in the $k_{I,max} - T_{start}$ plane. Resistance, reactance and impedance in the rated c) and starting d) operating point. Current density distribution of the optimal solutions in the rated e) and starting f) condition.

towards higher values. These statements are general and so valid independently from the considered cage material or slot area constraint; the relative contours are not reported for the sake of brevity.

- Higher starting torques are achieved thanks to the higher bar resistance and lower reactance at the same operating condition, as shown in Fig. 8c). The bar resistance and reactance at the starting condition have the same order of magnitude and for a given $k_{I,max}$, they are inversely proportional to each other. Therefore, moving along the iso-$k_{I,max}$ curve, the bar impedance at the starting does not drastically change. This behaviour is due to the non uniform current density distribution at the starting condition, reported in Fig. 8e). The latter creates the twofold effect: increasing the bar resistance and reducing its reactance. Such effect is emphasized as T_{start} increases and $k_{I,max}$ decreases. Consequently, it results in a longer bar neck (h_{in}) and in a reduced external bar circle (R_{out}).
- The rated efficiency trend in the $k_{I,max} - T_{start}$ plane can be justified analysing the rated bar resistance and reactance contour plots. As expected, being constant the slot area, the rated bar resistance does not vary in the $k_{I,max} - T_{start}$ plane. Consequently, it can be stated that the rated efficiency is mainly affected by the bar reactance variation. In fact, as the bar reactance decreases the efficiency increases. A similar correlation can be observed looking at the breakdown torque and the bar reactance at the same operating point. A decrements of the latter correspond to the enhancement of the breakdown torque. This confirm the common knowledge based on simplified analytical considerations that the T_{break} is inversely proportional to the rotor reactance and independent from the resistance [14]. However, it is worth to notice that a reduction of 85% (considering the extremes of the contour plots) of the reactance leads to a lower breakdown torque increment (≈70%); this implies that also the variation of R_{break} affects the breakdown torque. The correlation between X_{break} and T_{break} (and so also η_{rated}) is due to the fact that to reduce the starting current, the bar shape is transformed in such way that the leakage flux are enhanced (deep bars featuring small radius

of the bar's head). However, such leakage effect penalises the performance at low slips, when the current density is uniformly distributed (as shown in Fig. 8d)), thus requiring higher rated slip and therefore higher current to produce the same torque. When the starting current constraint is relaxed, higher efficiencies are achieved thanks to the more compact bar structure more exposed to the external periphery of the rotor. This permits to maintain high starting torque with reduced leakage inductance in favor of low rated slip values.

- An exception to the above considerations can be observed for low-$k_{I,max}$/high-T_{start}. In this region, at the rated condition, the bar resistance is higher while the reactance is unexpectedly lower. This is due to the non uniform current density distribution at the rated operating condition featured by the optimized slot labeled as $Al_{280}^{5.4}$ in Fig. 8d). This extreme case, caused by the constant slot area constraint, leads to high starting torque, limiting the respective current, without negatively affect the rated efficiency.

B. Comparison between optimal bars with fixed and variable area

In the following, the design solutions providing a starting torque of 160 Nm, optimized with and without the constraint of the slot area are compared. As shown Fig. 7 (blue continuous and dotted lines), more efficient designs are obtained with unlimited rotor bar cross section. In this cases the breakdown torque and the related slip are slightly reduced with respect to the solutions with constrained area. The same considerations related to the breakdown point are valid for all the combinations of $k_{I,max} - T_{start}$ and they are not reported for the sake of brevity. Regarding the geometries optimized unconstraining the slot area are simply a scaled version of the ones obtained limiting its surface, as shown in Fig. 7 (e.g. $Al_{160}^{5.4}$ and $Al_{160}^{*5.4}$). The above considerations are valid also for the optimal copper bars and they are not reported for the sake of brevity.

C. Comparison between optimal aluminium and copper bars with the same area

Comparing the results achieved fixing both $k_{I,max}$ and T_{start}, the only clear difference between the optimal copper and aluminium bars is related with the radius of the external circle (R_{out}). In particular, the copper bars present a R_{out} always smaller with respect to the aluminium ones. Considering that 1) the starting torque is roughly proportional to the bar resistance, 2) the external part of the cage is the most important in determining the starting performance, and 3) both bars have been optimizing considering the same area, it follows that the copper bar can provide the same T_{start} of the aluminium one only with a smaller radius of the outer circle R_{out} (ideally proportional to the ratio between the copper and aluminium resistivity). Analysing the torque-slip characteristics, for the same $k_{I,max}$ and T_{start}, the copper bar presents a lower breakdown torque at a lower slip with respect to the aluminium bar. The reduction of the breakdown slip can be surely ascribed to the lower resistivity of the copper and the higher leakage reactance of the optimized copper bar with respect to the aluminium ones. The lower breakdown torque of the copper bar is mainly due to the higher leakage reactance, while the resistance plays a minor role.

IV. Validation of the Optimization Method

In this section the proposed optimization procedure is further validated considering thermal management aspect and high orders harmonic losses. The first one is addressed via a coupled electromagnetic-thermal investigation while the second one is analysed carrying out voltage-fed time-step-with-motion FE simulations. These analysis enable to identify and quantify advantages and drawbacks of adopting an optimized copper cage with respect to aluminium cage.

A. Coupled electromagnetic-thermal analysis

All the optimizations presented so far are performed considering a constant temperature of the stator ($T_{sw0} = 80\,^{\circ}C$) and rotor ($T_{bar0} = 100\,^{\circ}C$) windings. Such assumption is introduced in order to simplify the iterative approach to compute the performance, thus reducing the computational effort. Although the bar geometry influences directly the losses, it has been reasonably assumed that the shape itself has a negligible direct effect upon the motor temperature distribution. In other words, given a certain value of losses, two very different bar shapes feature the same temperature rise. Consequently, re-evaluating the optimal solutions via a coupled electromagnetic-thermal analysis reaching the steady state temperature will surely modify the rated efficiencies but the optimality of the found solutions will be preserved. Fig. 9 shows the results of such multi-physics analysis carried out with FE simulations for both electromagnetic and thermal physics. In particular, the figure reports rated efficiencies, stator windings (T_{sw}) and rotor bars (T_{bar}) average temperatures for both aluminium and copper bars, optimized with unconstrained slot area. Although the Pareto fronts are not uniformly shifted, the optimality of the solutions is preserved for both aluminium and copper cages. In fact, major variations are exhibited by designs with high starting torques (and so low rated efficiency) which have higher losses at the rated operating point, thus feature higher temperature rise as shown by the T_{sw} and T_{bar} trends.
The adoption of copper bars allows to achieve higher efficiency with respect to the aluminium bars for low staring torque designs. The efficiency gain is about 0.4% in the best case, i.e. $k_{I,max} = 9.4$, and it reduces as the starting torque increases until it becomes negative for really high T_{start} and low $k_{I,max}$. In other words, the aluminium bars outperform the copper ones for designs requiring a very high starting torque with a low starting current. Similar trends are exhibited by the steady state temperatures of the stator windings and rotor bars. It is interesting to notice that for low starting torque and high k_I, when the copper cage is convenient with respect to the aluminium, a further advantage of the copper consists in a temperature reduction of the stator windings (≈ 8°C). The latter can be translated in a life time improvement of the insulation materials.

B. Voltage-fed time-step FE analysis

The approach to estimate the SCIM performance by adopting TH-FE simulations, to evaluate the parameters of the

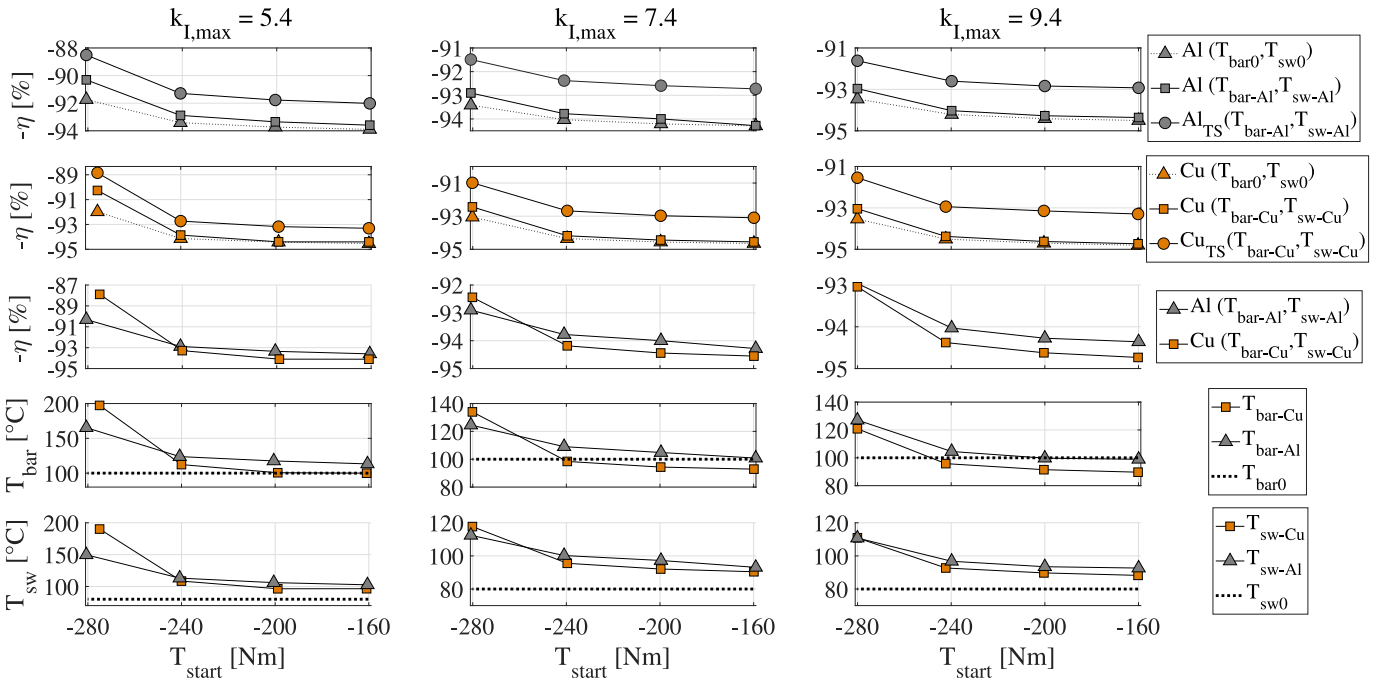

Fig. 9: Pareto fronts evaluated with fixed temperatures for the stator and rotor windings compared with the ones assessed at the correct steady state temperatures for the aluminium (first row) and copper (second row) cages. The third row shows the comparison between the optimal aluminium and copper bars at the correct temperatures. The last two rows reports the steady state bar and stator winding temperatures of all optimal solutions achieved unlimiting the slot area.

single-phase EC, has intrinsic limitations. Although it exhibits a very high accuracy in predicting the motor steady state characteristic, it is not able to consider high order harmonics of the stator and rotor currents. Therefore, variation of the losses (and so of the efficiency) are expected when such harmonic components are taken into account, being rotor joule losses and iron losses the most affected. Fig. 9 also reports the efficiencies of the optimal aluminium (Al_{TS}) and copper (Cu_{TS}) bars evaluated via a voltage-fed time step FEA so including the effect of such high order current harmonics. As expected, the efficiency has been overestimated during the design optimization, however the optimality of the solutions is preserved being the Pareto fronts uniformly shifted towards lower efficiency.

V. Conclusion

This work, second part of two companion papers, provides a complete analysis of the rotor slot design of SCIMs. It has been demonstrated that working on the rotor slot geometry it is possible to satisfy a very wide spectrum of requirements in terms of starting torque and current, while maintaining the highest rated efficiency. The selected objectives for the rotor optimization, rated efficiency, starting torque and respective current, show a clear competitive behaviour. In addition, it has been proved that the optimization of the rated efficiency implies the maximization of the rated power factor and breakdown and pull-up torques. The influence of the slot geometry on the EC rotor parameters and so on the SCIM performance have been deeply investigated. It has been established that adopting optimized copper bars is convenient for designs featuring low-medium starting torques. Instead, for applications demanding high starting capability, especially with a limited starting current, the aluminium cage is the preferred option. The outcomes of this work are defining a new approach to optimise the squirrel cage induction motor.

Acknowledgment

The authors gratefully acknowledge the financial support of ABB Corporate Research in Västerås.

References

[1] J. F. Fuchsloch, W. R. Finley, and R. W. Walter. The next generation motor. *IEEE Industry Applications Magazine*, 14(1):37–43, Jan 2008.
[2] A. T. De Almeida, F. J. T. E. Ferreira, and A. Q. Duarte. Technical and economical considerations on super high-efficiency three-phase motors. *IEEE Transactions on Industry Applications*, 50(2):1274–1285, 2014.
[3] IEC. Rotating electrical machines - part 30-1: Efficiency classes of line operated ac motors (ie code), 2014.
[4] A. Boglietti, A. Cavagnino, L. Ferraris, M. Lazzari, and G. Luparia. No tooling cost process for induction motors energy efficiency improvements. *IEEE Transactions on Industry Applications*, 41(3):808–816, May 2005.
[5] E. B. Agamloh, A. Boglietti, and A. Cavagnino. The incremental design efficiency improvement of commercially manufactured induction motors. *IEEE Transactions on Industry Applications*, 49(6):2496–2504, Nov 2013.
[6] L. Alberti, N. Bianchi, A. Boglietti, and A. Cavagnino. Core axial lengthening as effective solution to improve the induction motor efficiency classes. *IEEE Transactions on Industry Applications*, 50(1):218–225, Jan 2014.
[7] F. Parasiliti. Design strategies, new materials and technologies to improve induction motors efficiency. *Prace Instytutu Elektrotechniki*, Z. 223:27–42, 2005.
[8] A. Cavagnino, S. Vaschetto, L. Ferraris, Z. Gmyrek, E. B. Agamloh, and G. Bramerdorfer. Striving for the highest efficiency class with minimal impact for induction motor manufacturers. *IEEE Transactions on Industry Applications*, pages 1–1, 2019.
[9] A. Boglietti, A. Cavagnino, L. Feraris, and M. Lazzari. Energy-efficient motors. *IEEE Industrial Electronics Magazine*, 2(4):32–37, December 2008.

[10] W. R. Finley and M. M. Hodowanec. Selection of copper versus aluminum rotors for induction motors. *IEEE Transactions on Industry Applications*, 37(6):1563–1573, Nov 2001.
[11] Francesco Parasiliti and Marco Villani. *Design of High Efficiency Induction Motors with Die-Casting Copper Rotors*, pages 144–151. 01 2003.
[12] J. G. Cowie and D. T. Brender. Die-cast copper rotors for improved motor performance. In *Conference Record of the 2003 Annual Pulp and Paper Industry Technical Conference, 2003.*, pages 42–49, June 2003.
[13] Ali Canakoglu, Asım Yetgin, Hasan Temurtas, and Mustafa Turan. Induction motor parameter estimation using metaheuristic methods. *TURKISH JOURNAL OF ELECTRICAL ENGINEERING COMPUTER SCIENCES*, 22:1177–1192, 01 2014.
[14] I Boldea. *The Induction Machine Handbook*. 01 2002.

Mauro Di Nardo received the M.Sc.(Hons.) degree in electrical engineering from the Polytechnic University of Bari (Italy) in 2012, and the Ph.D. degree in electrical machine design from the University of Nottingham (UK) in 2017. From 2017 to 2019 he was head of the AROL research team within the Polytechnic University of Bari leading industrial R&D projects on electrical drives design for mechatronics applications. Since the 2019, he joined the Power Electronics and Machine Control Group of the University of Nottingham as Research Fellow. His research interests are the analysis, modelling, and optimizations of electrical machines, including permanent magnet and synchronous reluctance topologies for automotive and aerospace sectors as well as induction motor for industrial applications.

Alessandro Marfoli received the M.Sc. in Electrical Engineering from the University of Pisa, Italy, in 2015. He is actually working toward the PhD degree in electrical and electronic engineer at the Power Electronics, Machines and Control group, University of Nottingham, Nottingham, UK.

His main research interests include modelling, analysis and optimization of electrical machines.

Michele Degano (M'15) received his Master's degree in Electrical Engineering from the University of Trieste, Italy, in 2011, and his Ph.D. degree in Industrial Engineering from the University of Padova, Italy, in 2015. Between 2014 and 2016, he was a post-doctoral researcher at The University of Nottingham, UK, where he joined the Power Electronics, Machines and Control (PEMC) Research Group. In 2016 he was appointed Assistant Professor in Advanced Electrical Machines, at The University of Nottingham, UK. He was promoted Associate Professor in 2020. His main research focuses on electrical machines and drives for industrial, automotive, railway and aerospace applications, ranging from small to large power. He is currently the PEMC Director of Industrial Liaison leading research projects for the development of future hybrid electric aerospace platforms and electric transports.

Chris Gerada received the Ph.D. degree in numerical modeling of electrical machines from The University of Nottingham, Nottingham, U.K., in 2005. He was a Researcher with The University of Nottingham, working on high-performance electrical drives and on the design and modeling of electromagnetic actuators for aerospace applications. Since 2006, he has been the Project Manager of the GE Aviation Strategic Partnership. In 2008, he became a Lecturer in electrical machines, in 2011, as an Associate Professor, and in 2013, a Professor at The University of Nottingham. His main research interests include the design and modeling of high-performance electric drives and machines. Prof. Gerada serves as an Associate Editor for the IEEE TRANSACTIONS ON INDUSTRY APPLICATIONS and he is the Chair of the IEEE Industrial Electronic Society Electrical Machines Committee.

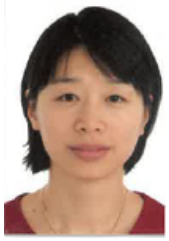

Wenliang Chen Wenliang Chen was born in 1986 (Shaanxi, China). She graduated from the Royal Institute of Technology and received her M. Sc. degree in Electrical Power Engineering in 2010. Since 2010 she has been with ABB Corporate Research (Sweden) as research scientist.

Her technical interest includes electromagnetic field analysis, high speed machines, winding losses from proximity effects.